Supporting Online Material for:

The Role of Trace Ag in the Synthesis of Au Nanorods

Liane M. Moreau[1,4], Matthew R. Jones[1,4], Eric W. Roth[1,4], Jinsong Wu[1,4], Sumit Kewalramani[1,4], Matthew N. O'Brien[2,4], Bor-Rong Chen[1], Chad A. Mirkin[1,2,4], and Michael J. Bedzyk[1,3,4]

[1]Department of Materials Science and Engineering, [2]Department of Chemistry, [3]Department of Physics and Astronomy, and [4]International Institute for Nanotechnology, Northwestern University, Evanston, IL 60208

Extended Methods

Nanorod Synthesis

According to the synthesis method established by El-Sayed and co-workers,[1] Au seed nanoparticles were synthesized by adding 0.6 mL of 0.01 M ice cold $NaBH_4$ (Sigma-Aldrich) to a stirring solution containing 5 mL 0.2 M CTAB (bioWORLD), 0.25 mL 0.01 M $HAuCl_4$ (Sigma-Aldrich) and 4.75 mL NANOpure™ water (18.2 MΩ.cm resistivity). In a separate vial, 5 mL 0.2 M CTAB, 0.3 mL 0.004 M $AgNO_3$ (Sigma-Aldrich), 0.5 mL 0.01 M $HAuCl_4$ and 4.5 mL NANOpure™ water were combined and 0.07 mL of 0.078 M ascorbic acid (Sigma-Aldrich) added to reduce Au^{3+} to Au^{+}. 0.012 mL of the as-synthesized seeds were added to this solution and reacted for 120 minutes to form the final nanorod product. It should be noted that in order to obtain sufficient sample with concentrations appropriate for XAFS measurements (micromolar concentrations of the element of interest within the nanopartices), the aforementioned synthesis volumes were scaled up as appropriate to a final reaction solution volume of up to 1 L. In order to quench the reaction, halting growth at timepoints prior to reaction completion, 100 mM bis(*p*-sulfonatophenyl)phenylphosphine (BSPP, Sigma Aldrich) was added to the nanorod growth solution to a final concentration of 2 mM. For ex-situ STEM measurements, nanorod were concentrated via high-speed centrifugation (21130 g) to form a pellet and re-suspended in 100 µL NANOpure™ water. For X-ray measurements, nanorods were concentrated to micromolar concentrations of Ag or Au atoms and washed several times with NANOpure™ water to remove excess reactant from solution. This ensured that

global average X-ray measurements were representative of the Ag and Au atoms within the nanoparticles rather than any excess which may remain in the growth solution.

STEM Size Analysis

Nanoparticle size was determined by a statistical analysis of TEM images using the ImageJ particle counter software. At least 100 particles were analyzed per timepoint aliquot in order to ensure a statistically meaningful sample population. Nanorod length and diameter were measured at the center of the tips and sides, respectively.

X-Ray Fluorescence

X-ray fluorescence (XRF) data from the Ag Kα and Au L fluorescence lines were collected along with XAFS data at sectors 10BM-B and 5 BM-D at the Argonne National Laboratory Advanced Photon Source (APS). The corrected fluorescence intensities of the Ag Kα and Au Lα lines were used to determine the relative Au and Ag atomic percentages present in the isolated nanoparticle samples quenched at various reaction timepoints. Samples were contained in 3 mm (nominal, Charles Supper) inner diameter cylindrical quartz capillaries placed such that the capillary long axis was at a 45° angle with the detector normal and the incident x-ray beam. The XRF photons were collected in the horizontal plane with the detector at ~ 90° relative to the incident beam direction to minimize the intensity due to elastically and inelastically scattered X-rays. XRF data was collected at an incident energy of 26.014 keV using a four-element Vortex ME-4 silicon drift diode detector.

Figure S1 shows a sample XRF spectrum. Quantitative analysis of the Au and Ag relative atomic percentages were conducted using areas under the Ag Kα (22.163 keV) and Au Lα (9.705 keV) fluorescence lines, with peaks fit to a Gaussian function after background subtraction. Elemental XRF cross sections,[2] detector efficiency, and attenuation due to solvent media were taken into account in determining the Ag/Au ratio. (Note that self-absorption by the metal NPs could be neglected due to their low μM atomic concentrations in the solvent.) The beam size was 0.4 mm (vertical) x 5 mm (horizontal). Therefore, for attenuation correction for Ag Kα and Au Lα X-rays coming from the 2 or 3

mm diameter cylinder of water, we neglected the vertical beam size. The path lengths and attenuation corrections for fluorescence X-rays were calculated by dividing the horizontal illuminated 14 - 21 mm^2 area into 121 differential emission elements arranged on a 2D lattice. The corrected intensities yielded the same atomic fraction for Au when Au Lα, Au Lβ or Au Lγ fluorescence lines were used, validating this correction procedure.

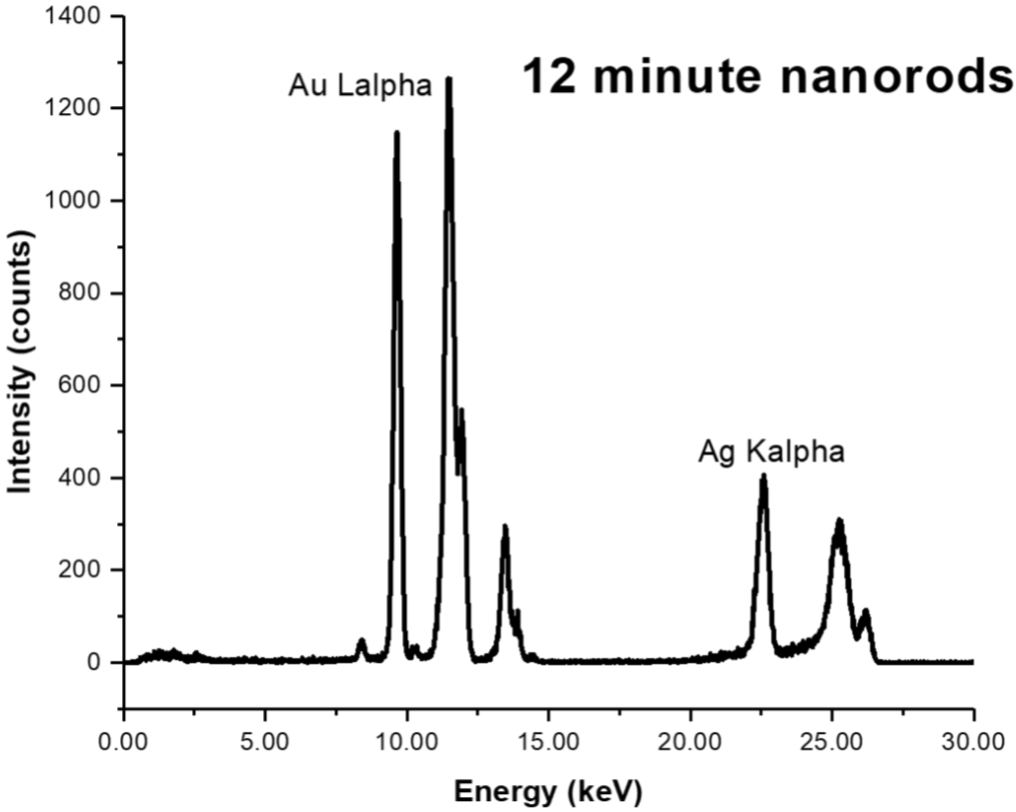

Figure S1. Sample X-Ray fluorescence spectrum. A sample XRF spectrum of the 12 minute nanorod aliquot is shown. The atomic % Ag and Au within the nanorods were determined from the corrected areas under the Au L alpha and Ag K alpha fluorescence lines (labeled). Lines other than the expected Au fluorescence lines between 10 and 15 keV are from Br present due to solution CTAB.

X-Ray Scattering

Small angle X-ray scattering (SAXS) measurements were performed using 10.00 keV X-rays at beamline 5ID-D of the Advanced Photon Source (APS) at the Argonne National Laboratory. The aqueous nanoparticle dispersions were placed in a quartz capillary tube (inner diameter ~ 1.5 mm). To avoid radiation damage, the sample was

translated in the beam to 5 nonoverlapping positions, from which the scattering patterns were averaged together. Furthermore, a fast shutter was used such that the samples were exposed to X-rays only for the data collection periods. The X-ray spot size at the sample position was ~ 0.25 mm (H) × 0.25 mm (V). The incident flux was ~ 10^{12} photons/s. The scattered intensity was collected using a Rayonix CCD area detector, which was placed at 7502.0 mm (range: q = 0.015 – 0.9 nm^{-1}) from the sample, where $q = 4\pi sin\theta/\lambda$ is the scattering vector magnitude defined by scattering angle, 2θ, and wavelength, λ. The flight path between the sample and detector was under vacuum.

For each nanoparticle sample, five 0.5 sec SAXS patterns were collected at each of the five spots. To account for fluctuations in the incident beam intensity and changes in the absorption of X-rays for different samples, the incident and the transmitted beam intensities were monitored using an ion chamber just before the sample and a pin diode embedded in the beam stop just in front of the SAXS detector. Transmission, detector solid angle and X-ray polarization corrections were applied to measured intensities before performing the azimuthal integration for extracting the 1D intensity profiles (figure S6).

X-Ray Absorption Fine Structure

XAFS spectra at the Au L_3 edge and Ag K edge (11.919 keV and 25.514 keV) were collected at MR-CAT sector 10BM-B of the APS. Energy scans were taken over a range from -150 eV to 600 eV with respect to the absorption edge using a Si(111) monochromator. XAFS spectra were collected in fluorescence mode using a four-element Vortex ME-4 Silicon drift diode fluorescence detector. The edge energies were calibrated with an Au or Ag metal foil standard. Ag or Au foil spectra were simultaneously collected along with the nanoparticle samples, as shown in Fig. S12, in order to ensure calibration and compare absorption edge positions. Samples were concentrated via centrifugation to μM concentrations of Au/Ag atoms and placed in 3 mm inner diameter quartz capillary tubes, positioned 45 degrees with respect to both the incident x-ray beam and the fluorescence detector. To improve statistics, a minimum of five half-hour scans at 4 spectra/scan were averaged. Self-absorption was not a concern in the measurement, because of the low concentration of the element of interest (Au or Ag).

XAFS data was processed using ATHENA and ARTEMIS software, part of the IFEFFIT package.[3] Theoretical crystals structures were imported and converted to scattering pathways using ATOMS.[4] Absorption edge energy was determined from the maximum of the first derivative in the absorption data and the background was subtracted using the AUTOBK algorithm.[5] The EXAFS region (greater than 100 eV above the absorption edge)[6] was normalized and a k-weight of 2 was chosen in order to provide an even spectrum throughout the region of interest (2 – 12 $Å^{-1}$). EXAFS spectra were modeled according to the EXAFS equation, a simplified version of which is:[6, 7, 8, 9]

$$\chi(k) = \sum_{\Gamma}\left[\frac{N_{\Gamma} S_0^2 F_{\Gamma}(k)}{2kR_{\Gamma}^2} e^{-2k^2\sigma_{\Gamma}^2} e^{-2R_{\Gamma}/\lambda(k)} \times \sin\left(2kR_{\Gamma} + \phi_{\Gamma}(k)\right)\right] \quad \text{(S1)}$$

Where Γ is the summation over the individual scattering pathways included in the model, *k* is the photoelectron wavevector, $F_\Gamma(k)$ is the scattering amplitude, λ(*k*) is the mean free path of inelastically-scattered photoelectrons and Φ(*k*) is the phase shift, which is calculated as a function of the absorbing and scattering atom using the ARTEMIS software. S_0^2, the amplitude reduction factor, was set to the value extracted from fitting a bulk Au or Ag foil as applicable. This enables a more accurate determination of the coordination number.[8] Degeneracy (N_Γ), half-path length (R_Γ), energy shift parameter (E_0), and mean-squared disorder (σ_Γ^2), which includes contributions from structural and thermal disorder (Debye-Waller factor),[6] were adjusted to determine the best fit model. Fits with values for these variables outside the realm of physical reasonability (e.g. negative mean-squared disorder) were rejected. ΔE_0 was fixed to a single variable for all pathways with the same absorbing and scattering element in order to limit the number of variables, as ΔE_0 values should be nearly equal for similar bonds within the structure.[10]

Goodness of fit parameters for the models were evaluated using minimization of the statistical R-factor parameter and error bars for individual parameters were estimated to one sigma (~ 68% confidence level) from the R-space spectrum. Spectra were fit first in k-space, then evaluated in R-space and q-space, in order to ensure that the best fit to the raw data in k-space was translatable to the other fitting spaces. Individual fitting models and a summary of both fitting and goodness of fit parameters are included in figure S12.

Sample Calculations

Calculation of Nanorod Growth Rates

Nanorod dimensions were determined from STEM analysis and are listed in table S1. As dimensions were determined as a function of reaction time, this enabled calculation of length, diameter and volume growth rates according to the following equation, where d is dimension, t_1 is time 1 and t_2 is time 2 :

$$growth\ rate = \frac{d_{t_1} - d_{t_2}}{t_1 - t_2} \quad \text{(S2)}$$

Growth rates were then plotted as a function of time. For example, to determine the nanorod length growth rate plotted at 10 minutes,

$$Length\ growth\ rate = \frac{23.1\ nm - 9.6\ nm}{12\ min. - 8\ min.}$$

$$Length\ growth\ rate = 3.4\ \frac{nm}{min.}$$

Calculation of Total Number of Ag Atoms per Nanorod

The total number of Ag atoms per nanorod (N_{Ag}) was calculated using nanorod volume (V_{rod}) determined from STEM dimensions, unit cell volume for FCC Au ($V_{u.c.}$), the number of atoms per unit cell (4) and the atomic fraction of Ag (F_{Ag}) in the nanorod determined from XRF:

$$N_{Ag} = \frac{V_{rod}}{V_{u.c.}} * 4 * F_{Ag} \quad \text{(S3)}$$

For example, for the 8 minute nanorod aliquot:

$$N_{Ag} = \frac{378\ nm^3}{0.0678\ nm^3} * 4 * 0.091$$

$$N_{Ag} = 2027 \pm 328$$

Calculation of % Ag in Nanorods that is on the Nanorod Surface

Coordination numbers (CNs) extracted from EXAFS analysis were used to determine the fraction (x_{Ag}) of Ag atoms in the nanorods that are on the nanorods surfaces. CN_{Ag} = 12 would indicate all Ag are in the bulk of the nanorod, i.e. x_{Ag} =0. Whereas, CN_{Ag} <12 indicates that x_{Ag} >0. At 8 mins we measured CN_{Ag} = 7.8, which indicates that surface Ag must be mostly on {110} surfaces since this surface has the low CN of 7 (< CN_{Ag}). Therefore, if we assume that surface Ag have CN = 7 and nonsurface Ag have CN =12 then

$$x_{Ag} = \frac{12 - CN_{Ag}}{5} \quad \text{(S4)}$$

For example, at 8 mins. when CN = 7.8, x_{Ag} = *0.84 ± 0.07.*

Note that Ag surface coverage Θ_{Ag} is the fraction of nanorod surface atoms that are Ag. Whereas, x_{Ag} is the fraction of Ag atoms in the nanorod that are on the nanorod surface.

Calculation of {110} Ag surface coverage

Ag {110} surface coverage (Θ_{Ag}) was calculated from x_{Ag} the fraction of Ag in the nanorods that is on the surface (see above calculation), the total number of Ag atoms in the nanorods (N_{Ag}, see above calculation) and the total number of atoms (Ag and Au) on the nanorod {110} surfaces ($N_{total,\{110\}}$) assumed as number of atoms on surface area of the sides of the nanorods, since the sides of the rods have been found to be {110}).[11] $N_{total,\{110\}}$ was calculated from the area of the side faces of the nanorods ($A_{\{110\}}$) and the number density of atoms for the {110} plane (σ_{110}). For FCC Au, which has a lattice parameter of 0.408 nm, σ_{110} = 8.501 nm^{-2}

$$N_{total,\{110\}} = (A_{\{110\}} * \sigma_{110}) \quad \text{(S5)}$$

$$\Theta_{Ag} = \frac{N_{Ag} * x_{Ag}}{N_{total,\{110\}}} \quad \text{(S6)}$$

For example, for the 8 min. nanorod sample,

$$N_{total,\{110\}} = (A_{\{110\}} * \sigma_{110})$$

$$N_{total,\{110\}} = (241\ nm^2 * 8.501\ nm^{-2})$$

$$N_{total,\{110\}} = 2049 \pm 613$$

$$\Theta_{Ag} = \frac{N_{Ag} * x_{Ag}}{N_{total,\{110\}}}$$

$$\Theta_{Ag} = \frac{2027 * 0.84}{2049}$$

$$\Theta_{Ag} = 0.83 \pm 0.26$$

Calculations for the case that the nanorod elongated surfaces are {520} rather than {110} facets

For the purpose of the manuscript, we assume that the sides of the nanorods are in majority {110} facets, as has been previously reported. There are studies, however, that claim the surface facets are instead {520}.[12-14] To see how the choice of this alternative surface facet affects the trend of our results, we have also calculated the Ag surface coverage for the case that the surface facets are {520} and plotted the results below, which can be compared to Figure 5b from the manuscript.

If we assume that surface Ag have CN = 6 (CN of a {520} surface atom) and nonsurface Ag have CN =12 then

$$x_{Ag} = \frac{12 - CN_{Ag}}{6}$$

For example, at 8 mins. when CN = 7.8, $x_{Ag} = 0.7$.

Ag {520} surface coverage (Θ_{Ag}) was calculated from x_{Ag} the fraction of Ag in the nanorods that is on the surface (see above calculation), the total number of Ag atoms in the nanorods (N_{Ag}, see above calculation) and the total number of atoms (Ag and Au) on the nanorod {520} surfaces ($N_{total,\{520\}}$) assumed as number of atoms on surface area of the sides of the nanorods, for the case that the sides of the nanorods are {520}. $N_{total,\{520\}}$ was calculated from the area of the side faces of the nanorods ($A_{\{520\}}$) and the number

density of atoms for the {520} plane (σ_{520}). For FCC Au, which has a lattice parameter of 0.408 nm, σ_{520} = 4.55 nm^{-2}, which is lower than the case for {110} given that {520} is a higher-index, more open facet than is {110}.

$$N_{total,\{520\}} = (A_{\{520\}} * \sigma_{520})$$

$$\Theta_{Ag} = \frac{N_{Ag} * x_{Ag}}{N_{total,\{250\}}}$$

For example, for the 8 min. nanorod sample,

$$N_{total,\{520\}} = (A_{\{520\}} * \sigma_{520})$$

$$N_{total,\{520\}} = (241\ nm^2 * 4.55\ nm^{-2})$$

$$N_{total,\{520\}} = 1097$$

$$\Theta_{Ag} = \frac{N_{Ag} * x_{Ag}}{N_{total,\{520\}}}$$

$$\Theta_{Ag} = \frac{2027 * 0.7}{1097}$$

$$\Theta_{Ag} = 1.29 \pm 0.39$$

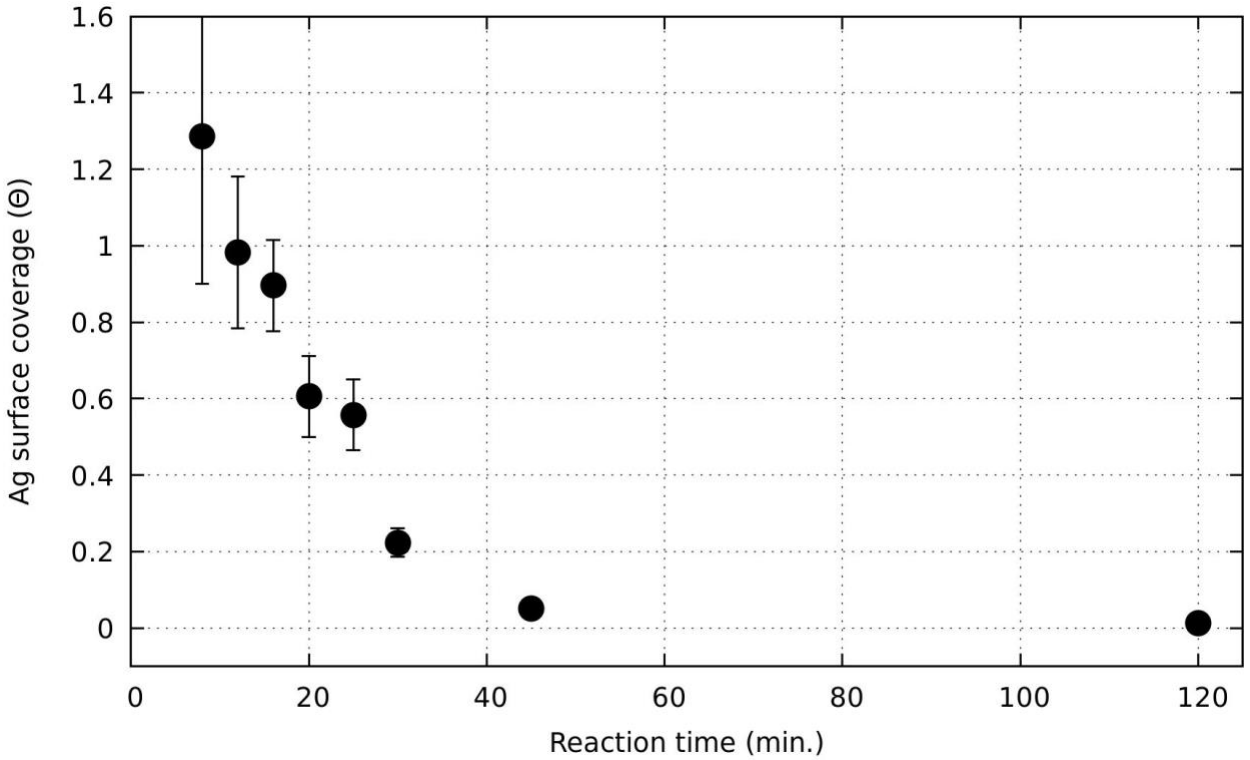

Figure S2. Ag surface coverage over time calculated assuming Ag is on {520} facets. When we compare the above figure to figure 5b, where surface coverage is calculated assuming Ag is on {110} facets, we see that the overall trend in the calculated Ag surface coverage is the same. Therefore, our Ag distribution results are valid independent of the assumption of facet identity.

Supplementary Results

L and W Dimensions from STEM analysis. Assumed $V_{rod} = LW^2$ and $A_{110} = 4LW$

Time (minutes)	Length (nm)	Width (nm)	Aspect ratio
8	9.6 ± 2.5	6.3 ± 0.9	1.5 ± 0.5
12	23.1 ± 3.9	6.3 ± 0.7	3.6 ± 0.7
16	33.6 ± 3.5	8.0 ± 0.7	4.2 ± 0.6
20	34.7 ± 4.5	9.0 ± 1.0	3.8 ± 0.7
25	43.1 ± 4.8	11.2 ± 1.4	3.9 ± 0.6
30	48.0 ± 5.4	12.2 ± 1.5	3.9 ± 0.7
45	50.9 ± 5.3	13.7 ± 1.9	3.7 ± 0.6
120	54.4 ± 4.4	14.9 ± 1.4	3.7 ± 0.4

Table S1. Dimensions determined from STEM analysis. Length and width determined from statistical analysis of STEM images and the determined aspect ratio of the nanorods for aliquots taken as a function of reaction time from 8 to 120 minutes.

Nanorod Dimension Evolution

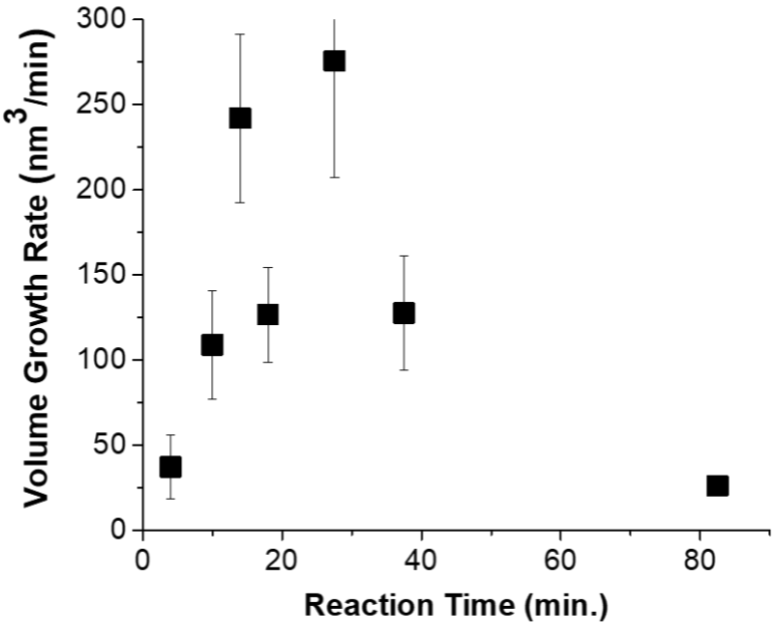

Figure S3. Nanorod volume growth rate. Volume growth rate as determined from STEM dimensions as a function of reaction time.

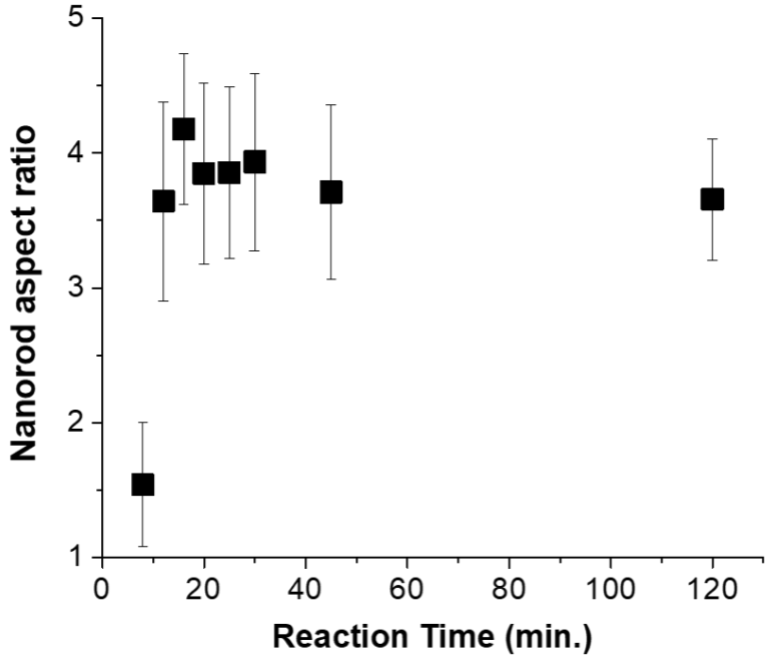

Figure S4. Nanorod aspect ratio. Nanorod aspect ratio as determined from STEM dimensions as a function of reaction time.

Evaluation of BSPP as an exchange ligand

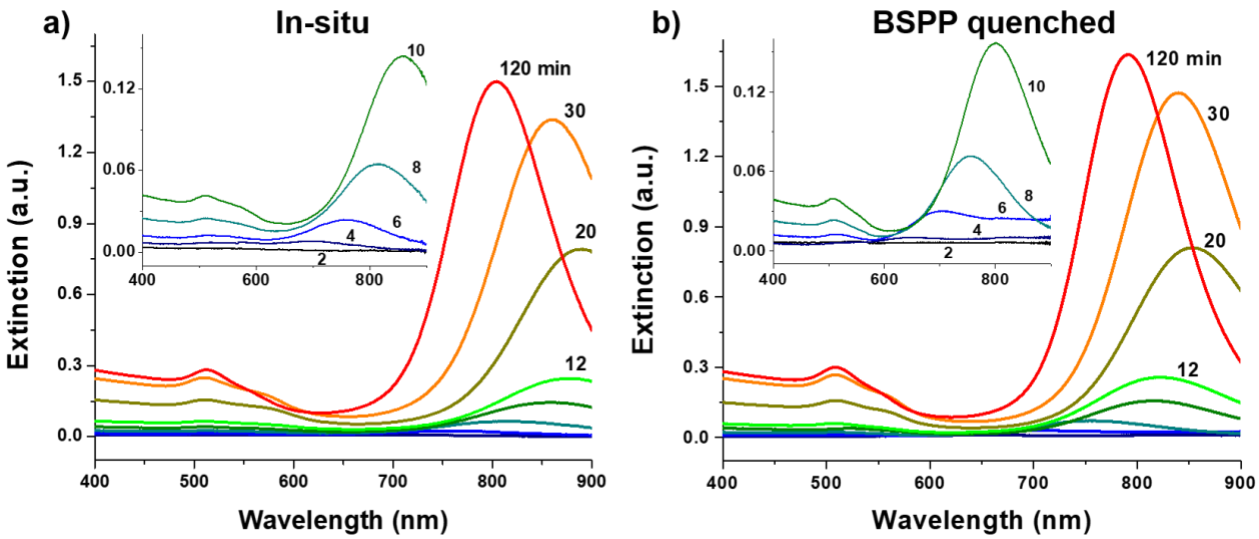

Figure S5. UV-vis spectra for nanorods synthesized in-situ and quenched with BSPP. To confirm that BSPP quenching does not affect the nanorod structure, UV-vis spectra were collected during the same synthesis reaction in-situ (left) and quenched with BSPP (right) at varying timepoints throughout the course of the synthesis reaction. It is observed that the spectral trends remain the same for the BSPP-quenched as for the in-situ samples, indicating that the nanorod morphology is unaffected by quenching with BSPP. The slight blue-shift observed for the BSPP-quenched samples compared to in-situ samples of the same timepoint is uniform throughout the reaction and expected due to the sensitivity of UV-vis signatures to the surrounding dielectric environment.[15]

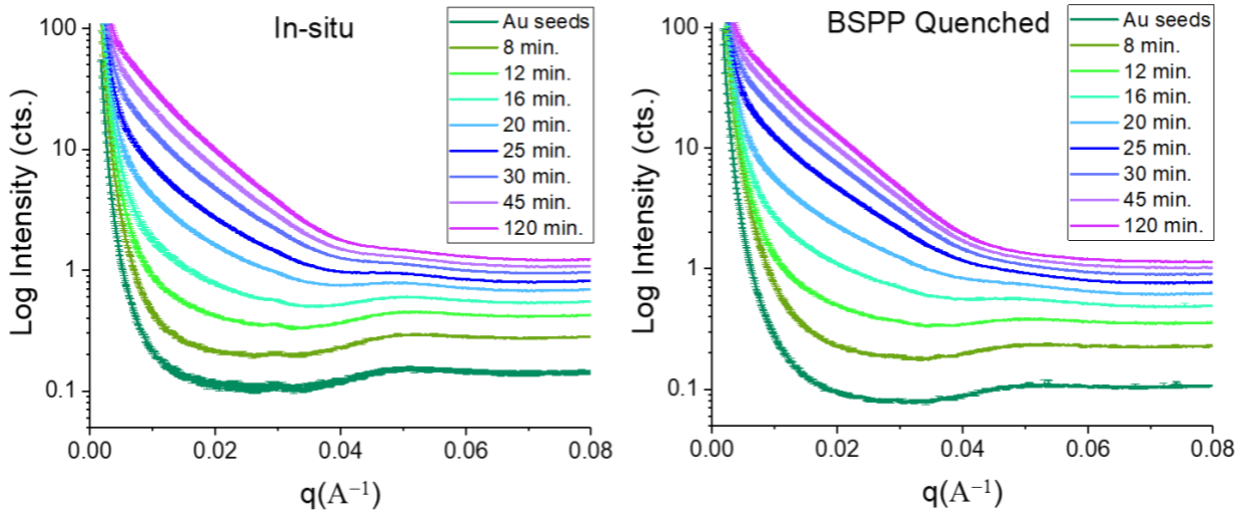

Figure S6. SAXS 1-D intensity profiles for nanorods synthesized in-situ and quenched with BSPP. SAXS patterns were collected during the same synthesis reaction in-situ (left) and quenched with BSPP (right) at varying timepoints throughout the course of the synthesis reaction. The observed trends are consistent between in-situ and ex-situ samples.

XANES Results

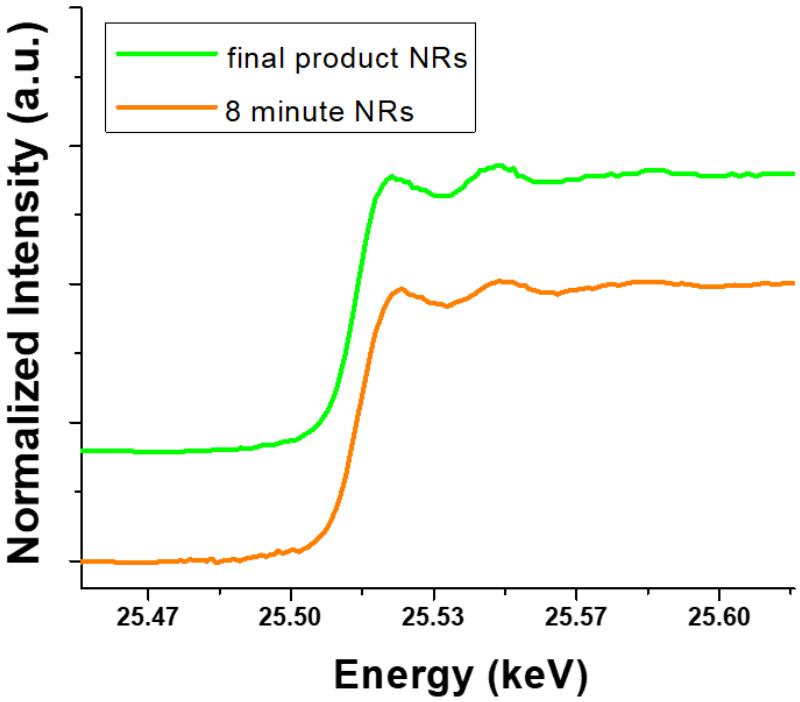

Figure S7. Nanorod XANES spectra. From the near edge region of the XAFS spectra, in comparison to Ag^{+} and Ag^{0} standards it was determined that the Ag in the final product nanorods (green) is Ag^{0}. The XANES spectrum of the 8 minute nanorods (orange), when most of the Ag is on the nanorod surface, is identical to that of the final product nanorods. This indicates that Ag is in the Ag^{0} state throughout the course of the reaction, even when Ag resides on the nanorod surface. This is in agreement with what is expected for Ag UPD.[11, 16]

XAFS-derived Results

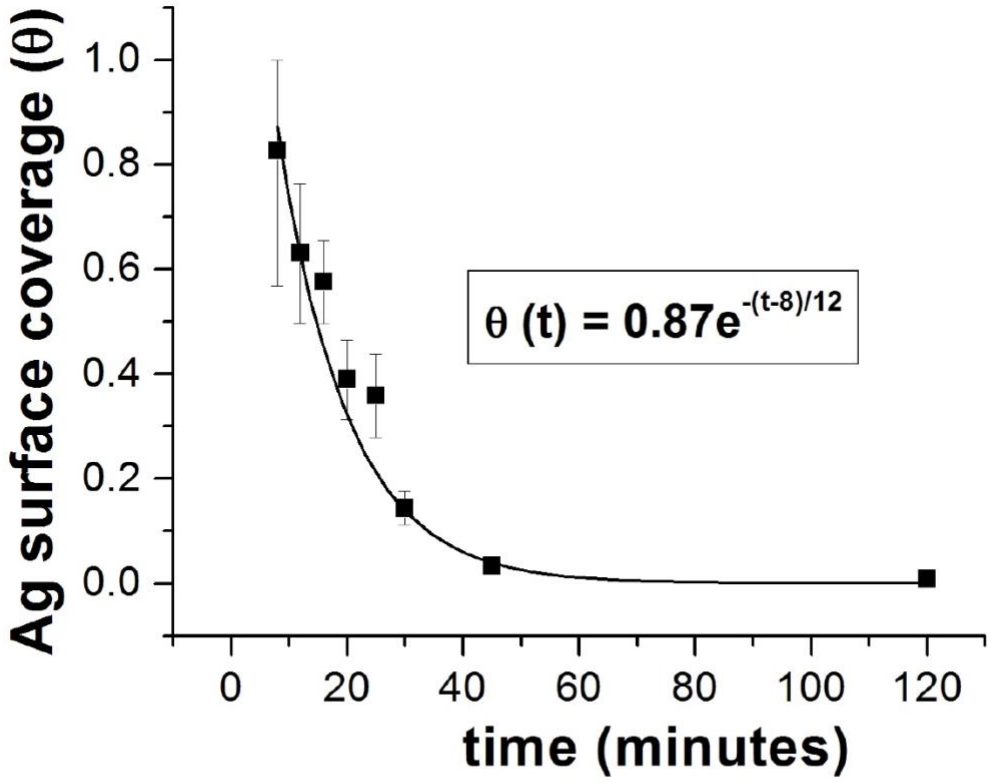

Figure S8. Exponential decay fit to data for Ag surface coverage vs. time. The displayed equation determined from the fit was used to obtain Ag surface coverage values at the mid-points for nanorod growth rate value determination, such that the Ag surface coverage and nanorod growth rates could be plotted together in Fig. 8.

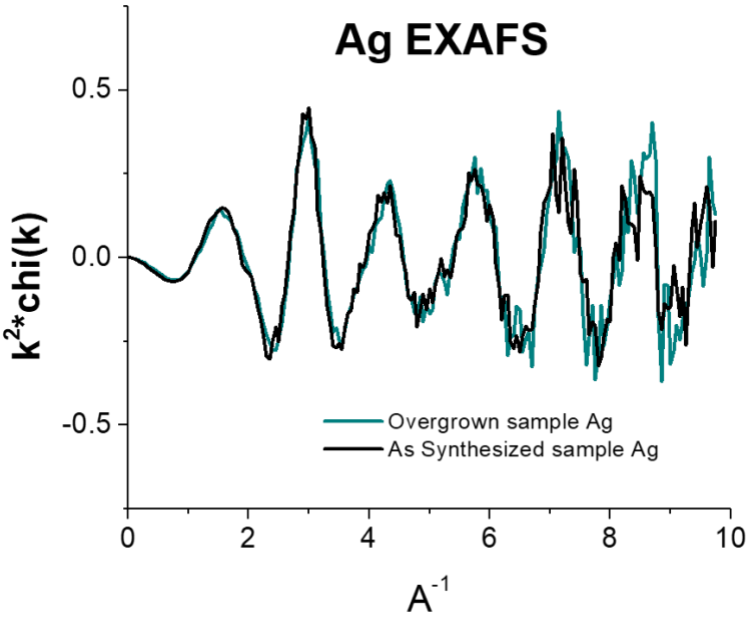

Figure S9. EXAFS k-space spectra of final product nanorods and final product nanorods overgrown with an Au shell. The k-space Ag K-edge EXAFS spectra of as-synthesized nanorods (black) and these same nanorods overgrown with an Au shell (teal) are identical. The overgrowth should encapsulate any surface Ag. If Ag were on the surface of the final product nanorods, differences between these two spectra should be apparent, due to differences in the coordination environment. If the Ag is already incorporated into the nanorod interior, however, the two spectra should be identical, which is the observed result.

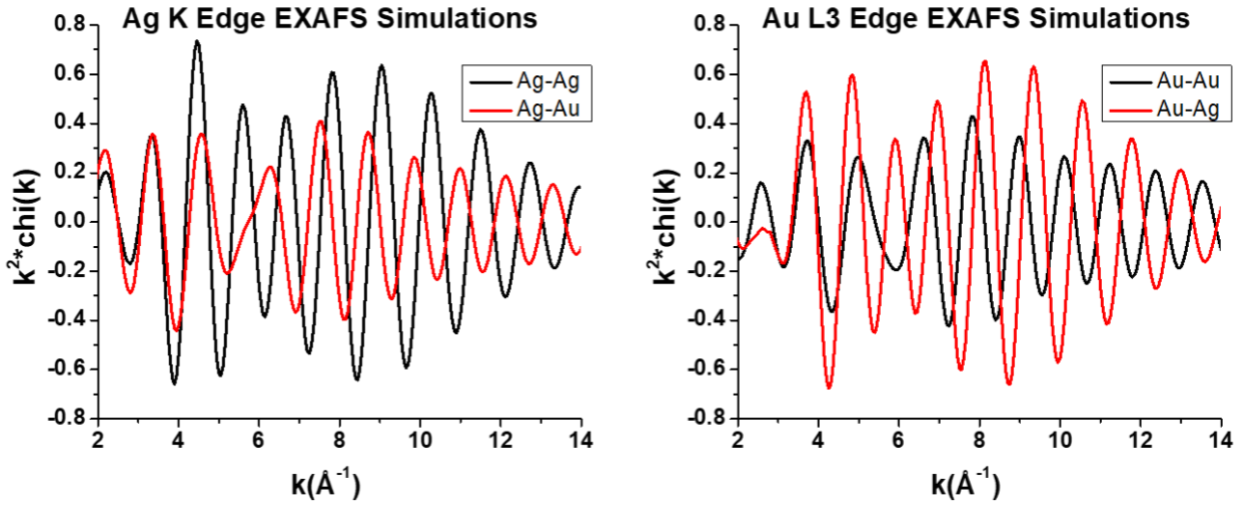

Figure S10. EXAFS Ag K edge and Au L3 edge simulations. Simulations of the Ag K-edge (left) and Au L3 edge (right) for different first-shell scattering atoms (Ag vs. Au) are shown. Major differences are observed in both the period of the oscillations as well as their amplitude as a function of k. Thus the contributions from the different scatterers can be extracted reliably through quantitative analysis

.

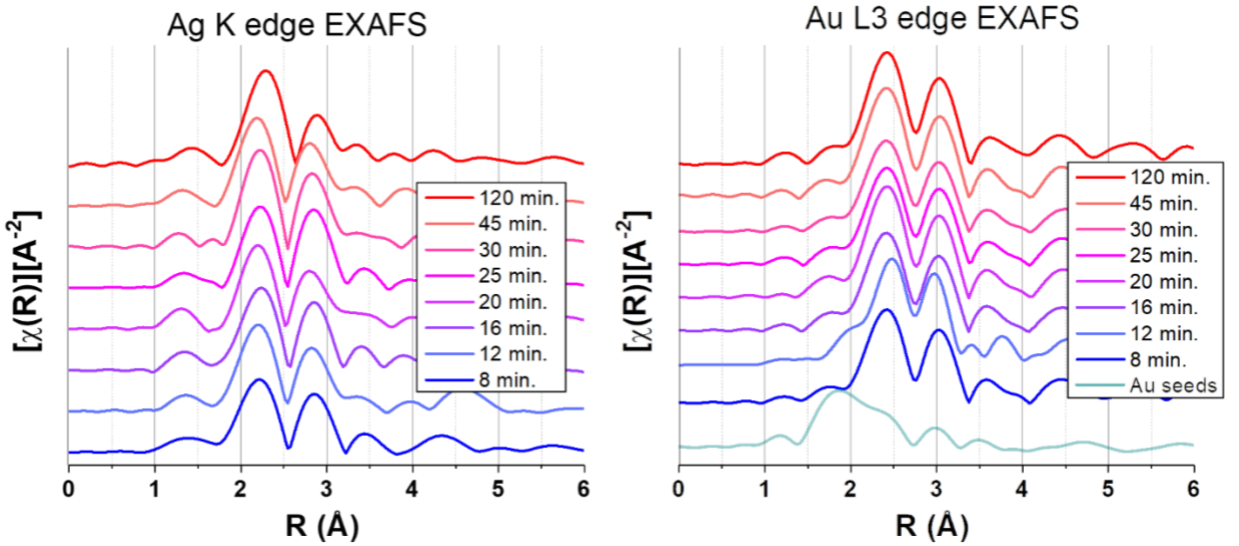

Figure S11. EXAFS Ag K edge and Au L3 edge data as a function of reaction time. Ag K edge EXAFS spectra (left) and Au L3 edge EXAFS spectra (right) are plotted with vertical offsets in a gradient from 8 minutes (blue) to final product nanorods (red).

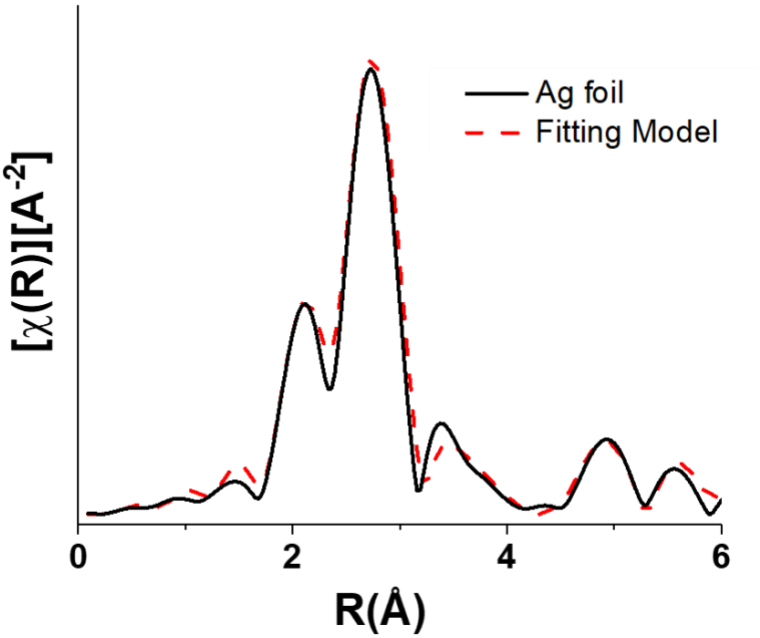

Pathway	N_{theory}	S_0^2	R (Å)	E_0 (eV)	σ^2 (Å^2) x 10^{-3}
Ag–Ag (shell 1)	12	0.74	2.866	2.35	8.03
Ag–Ag (shell 2)	6	0.74	4.062	2.35	9.85
Ag–Ag (shell 3)	24	0.74	5.009	2.35	12.1

Figure S12.1 Ag foil standard and fitting model. Ag foil data was collected and modeled in order to determine the amplitude reduction factor (S_0^2), since the coordination number is a fixed known. A fitting range from 1.5 to 5 Å and a k-range from 2 to 12 Å^{-1} was used. The R-factor parameter associated with the goodness of fit for this model was 0.034.

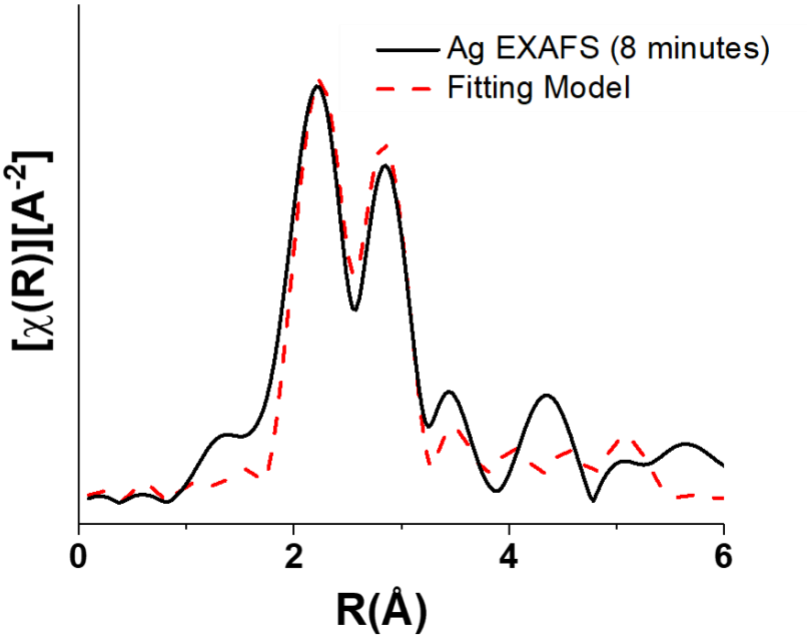

Pathway	N	R (Å)	E_0 (eV)	σ^2 (Å^2) x 10^{-3}
Ag–Ag (shell 1)	1.2 ± 0.2	2.83 ± 0.02	-8.1 ± 1.4	9.2 ± 2.1
Ag–Au (shell 1)	6.6 ± 0.6	2.865 ± 0.008	0.1 ± 0.4	12.5 ± 1.5

Figure S12.2 Ag K edge EXAFS spectrum and fitting model for 8 minute nanorod aliquot. The Ag K-edge nanoparticle spectrum was fit using first coordination-shell atomic pathways. A fitting range from 1.5 to 4 Å and a k-range from 2 to 10 Å^{-1} was used. The R-factor parameter associated with the goodness of fit for this model was 0.039.

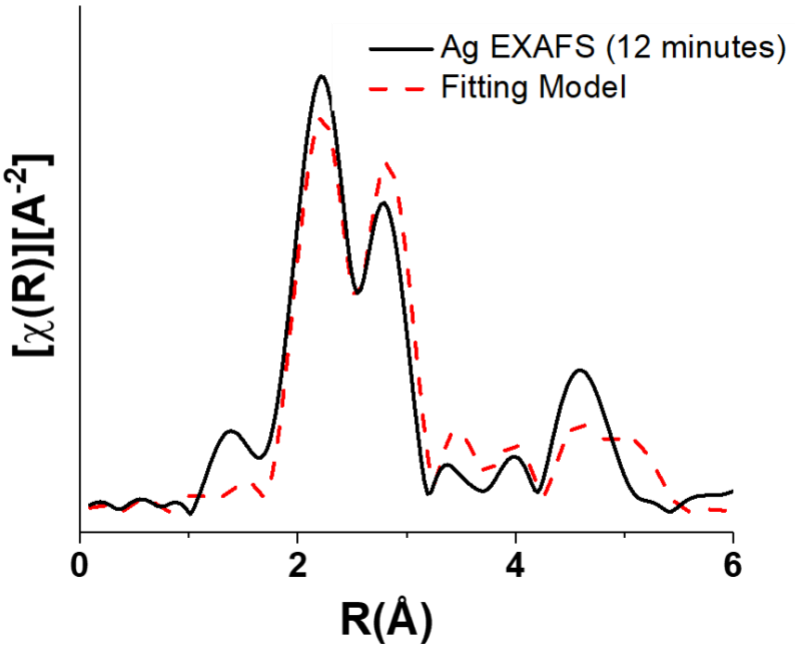

Pathway	N	R (Å)	E_0 (eV)	σ^2 (Å^2) x 10^{-3}
Ag–Ag (shell 1)	1.3 ± 0.2	2.83 ± 0.01	-7.9 ± 1.4	8.0 ± 1.2
Ag–Au (shell 1)	7.4 ± 0.5	2.865 ± 0.006	-0.2 ± 0.4	12.6 ± 0.8

Figure S12.3 Ag K edge EXAFS spectrum and fitting model for 12 minute nanorod aliquot. The Ag K-edge nanoparticle spectrum was fit using first coordination-shell atomic pathways. A fitting range from 1.5 to 4 Å and a k-range from 2 to 10 Å^{-1} was used. The R-factor parameter associated with the goodness of fit for this model was 0.035.

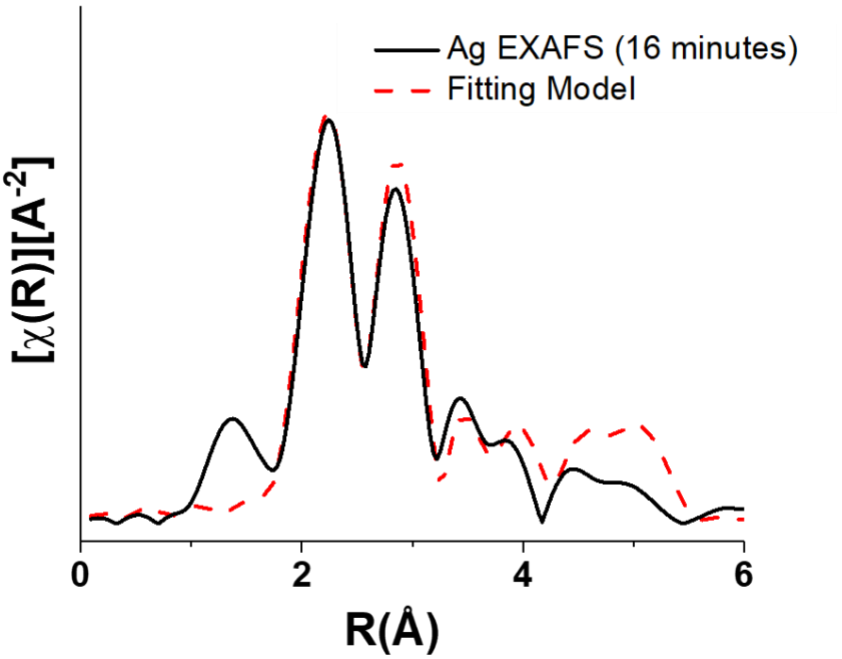

Pathway	N	R (Å)	E_0 (eV)	σ^2 (Å^2) x 10^{-3}
Ag–Ag (shell 1)	1.2 ± 0.1	2.83 ± 0.01	-4.8 ± 1.2	7.5 ± 1.3
Ag–Au (shell 1)	8.2 ± 0.3	2.863 ± 0.005	0.5 ± 0.3	12.4 ± 0.7

Figure S12.4 Ag K edge EXAFS spectrum and fitting model for 16 minute nanorod aliquot. The Ag K-edge nanoparticle spectrum was fit using first coordination-shell atomic pathways. A fitting range from 1.5 to 4 Å and a k-range from 2 to 10 Å^{-1} was used. The R-factor parameter associated with the goodness of fit for this model was 0.028.

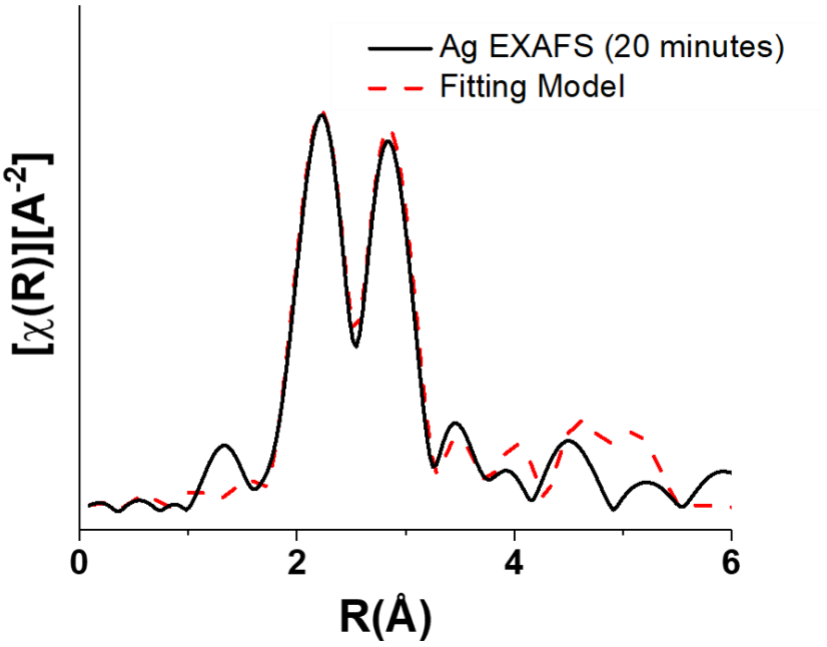

Pathway	N	R (Å)	E_0 (eV)	σ^2 (Å^2) x 10^{-3}
Ag–Ag (shell 1)	1.6 ± 0.4	2.829 ± 0.008	-6.8 ± 1.0	7.5 ± 2.4
Ag–Au (shell 1)	8.3 ± 0.8	2.865 ± 0.005	0.7 ± 0.3	12.5 ± 1.2

Figure S12.5 Ag K edge EXAFS spectrum and fitting model for 20 minute nanorod aliquot. The Ag K-edge nanoparticle spectrum was fit using first coordination-shell atomic pathways. A fitting range from 1.5 to 4 Å and a k-range from 2 to 10 Å^{-1} was used. The R-factor parameter associated with the goodness of fit for this model was 0.028.

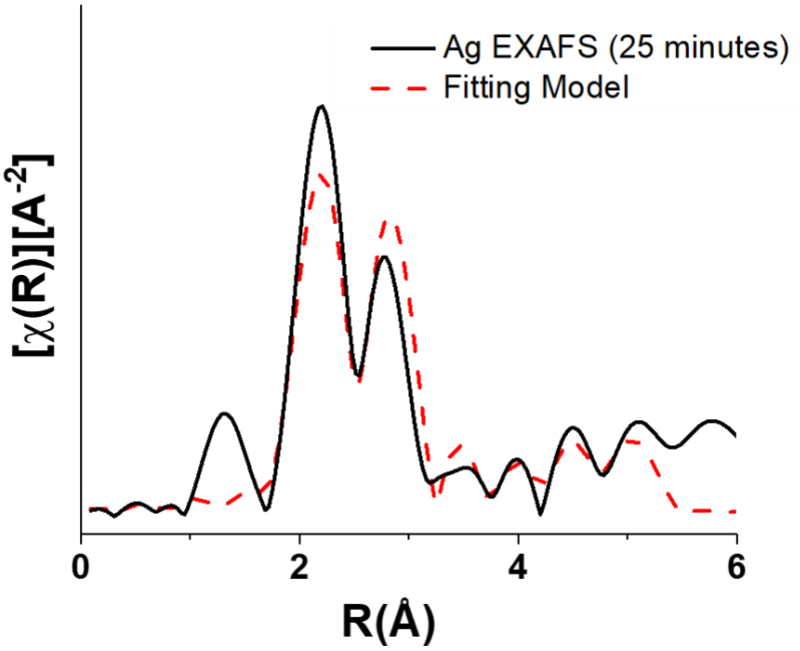

Pathway	N	R (Å)	E_0 (eV)	σ^2 (Å^2) x 10^{-3}
Ag–Ag (shell 1)	1.2 ± 0.3	2.82 ± 0.02	-8.7 ± 3.7	7.4 ± 3.6
Ag–Au (shell 1)	8.5 ± 1.4	2.87 ± 0.01	-0.4 ± 0.5	14.4 ± 2.6

Figure S12.6 Ag K edge EXAFS spectrum and fitting model for 25 minute nanorod aliquot. The Ag K-edge nanoparticle spectrum was fit using first coordination-shell atomic pathways. A fitting range from 1.5 to 4 Å and a k-range from 2 to 10 Å^{-1} was used. The R-factor parameter associated with the goodness of fit for this model was 0.038.

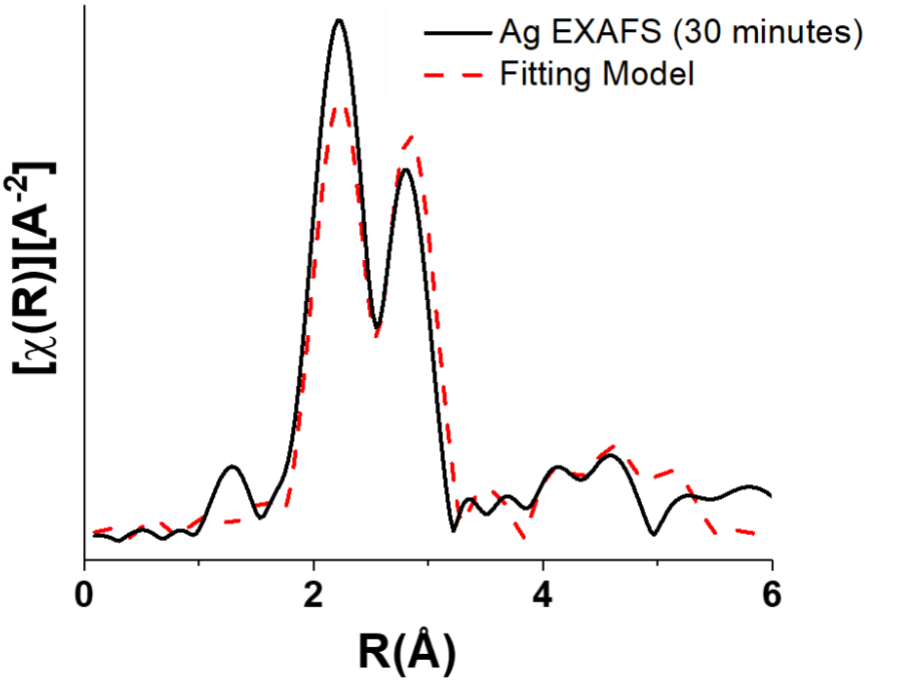

Pathway	N	R (Å)	E_0 (eV)	σ^2 (Å^2) x 10^{-3}
Ag–Ag (shell 1)	1.5 ± 0.3	2.85 ± 0.02	-6.4 ± 3.9	7.3 ± 2.9
Ag–Au (shell 1)	9.3 ± 1.6	2.87 ± 0.01	0.8 ± 0.7	14.0 ± 3.0

Figure S12.7 Ag K edge EXAFS spectrum and fitting model for 30 minute nanorod aliquot. The Ag K-edge nanoparticle spectrum was fit using first coordination-shell atomic pathways. A fitting range from 1.5 to 4 Å and a k-range from 2 to 10 Å^{-1} was used. The R-factor parameter associated with the goodness of fit for this model was 0.047.

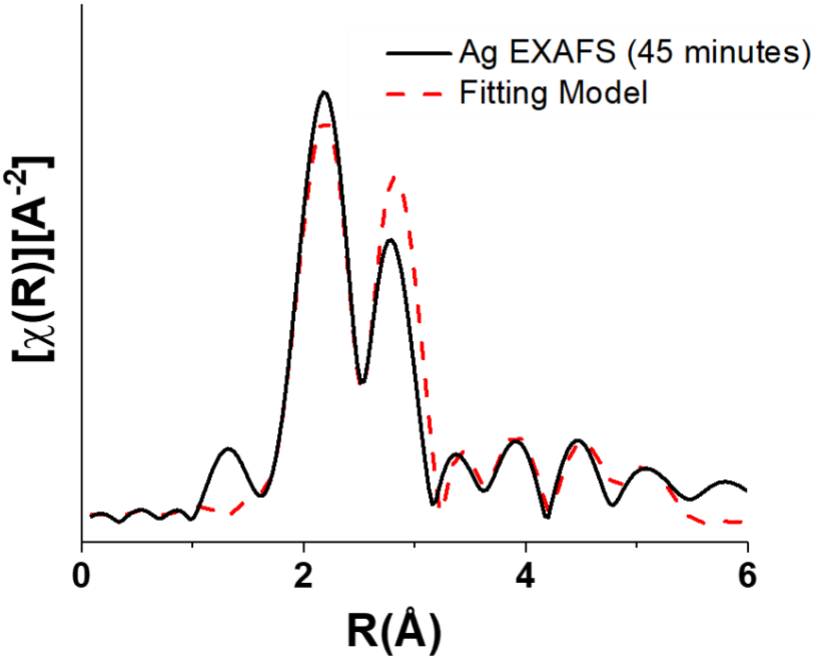

Pathway	N	R (Å)	E_0 (eV)	σ^2 (Å^2) x 10^{-3}
Ag–Ag (shell 1)	1.3 ± 0.3	2.82 ± 0.02	-8.9 ± 3.5	7.3 ± 1.6
Ag–Au (shell 1)	10.2 ± 1.5	2.87 ± 0.01	-1.3 ± 0.7	14.1 ± 2.8

Figure S12.8 Ag K edge EXAFS spectrum and fitting model for 45 minute nanorod aliquot. The Ag K-edge nanoparticle spectrum was fit using first coordination-shell atomic pathways. A fitting range from 1.5 to 4 Å and a k-range from 2 to 10 Å^{-1} was used. The R-factor parameter associated with the goodness of fit for this model was 0.048.

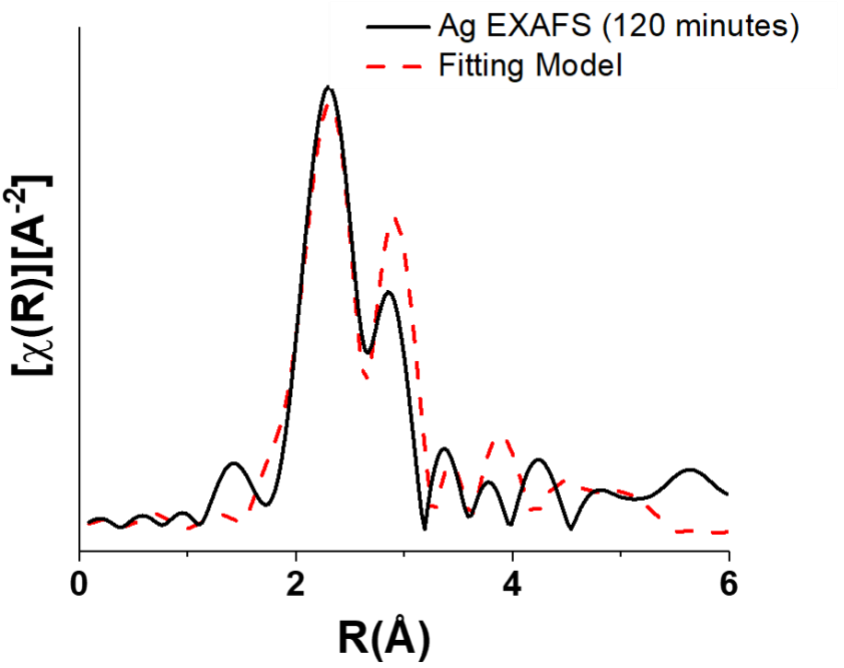

Pathway	N	R (Å)	E_0 (eV)	σ^2 (Å^2) x 10^{-3}
Ag–Ag (shell 1)	0.4 ± 0.4	2.83 ± 0.03	-3.0 ± 3	15.3 ± 5.2
Ag–Au (shell 1)	11.6 ± 1.4	2.89 ± 0.01	-1.2 ± 0.8	14.4 ± 1.9

Figure S12.9 Ag K edge EXAFS spectrum and fitting model for 120 minute final nanorod product. The Ag K-edge nanoparticle spectrum was fit using first coordination-shell atomic pathways. A fitting range from 1.5 to 4 Å and a k-range from 2 to 10 Å^{-1} was used. The R-factor parameter associated with the goodness of fit for this model was 0.1.

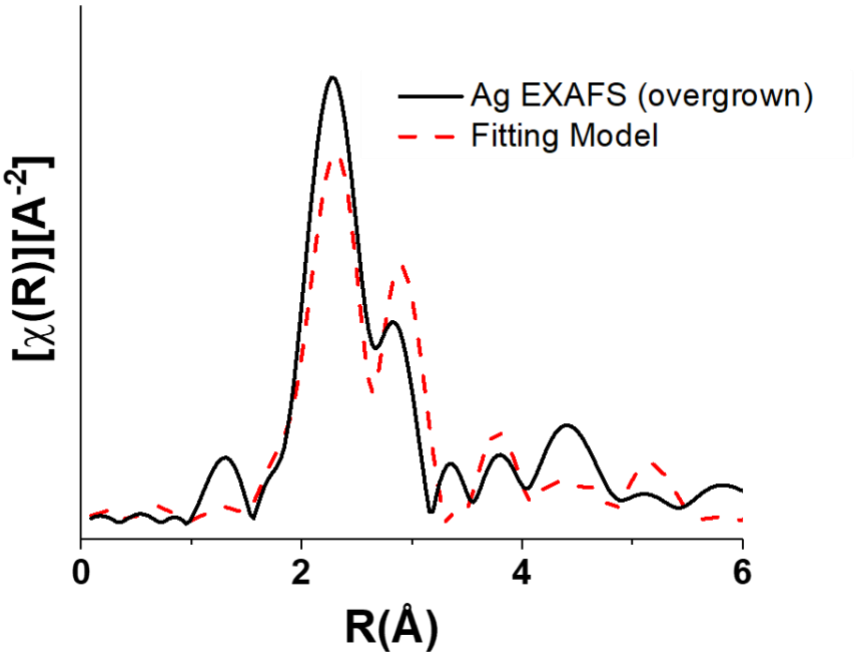

Pathway	N	R (Å)	E_0 (eV)	σ^2 (Å^2) x 10^{-3}
Ag–Ag (shell 1)	0.7 ± 1.3	2.81 ± 0.05	-4.1 ± 1.5	13.9 ± 4.2
Ag–Au (shell 1)	11.8 ± 1.7	2.88 ± 0.01	-1.1 ± 1.1	14.3 ± 2.4

Figure S12.10 Ag K edge EXAFS spectrum and fitting model for Au-overgrown nanorods. The Ag K-edge nanoparticle spectrum was fit using first coordination-shell atomic pathways. A fitting range from 1.5 to 4 Å and a k-range from 2 to 10 Å^{-1} was used. The R-factor parameter associated with the goodness of fit for this model was 0.15.

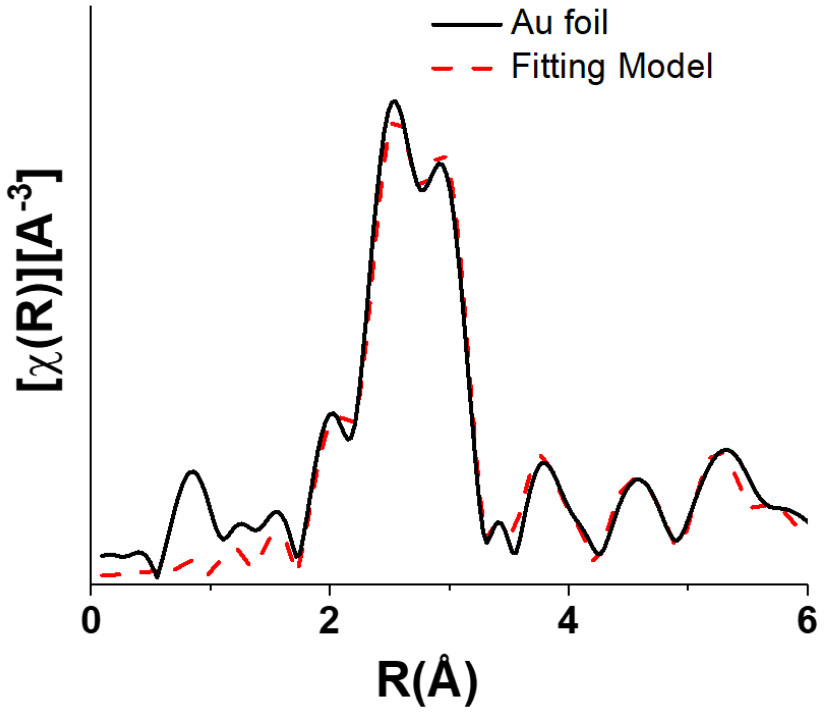

Pathway	N_{theory}	S_0^2	R (Å)	E_0 (eV)	σ^2 (Å^2) x 10^{-3}
Au–Au (shell 1)	12	0.75	2.861	5.11	7.71
Au–Au (shell 2)	6	0.75	4.051	5.11	10.8
Au–Au (shell 3)	24	0.75	4.986	5.11	12.0

Figure S12.11 Au foil standard and fitting model. Au foil data was collected and modeled in order to determine the amplitude reduction factor (S_0^2), since the coordination number is a fixed known. A fitting range from 1.5 to 5 Å and a k-range from 2 to 12 Å^{-1} was used. The R-factor parameter associated with the goodness of fit for this model was 0.034.

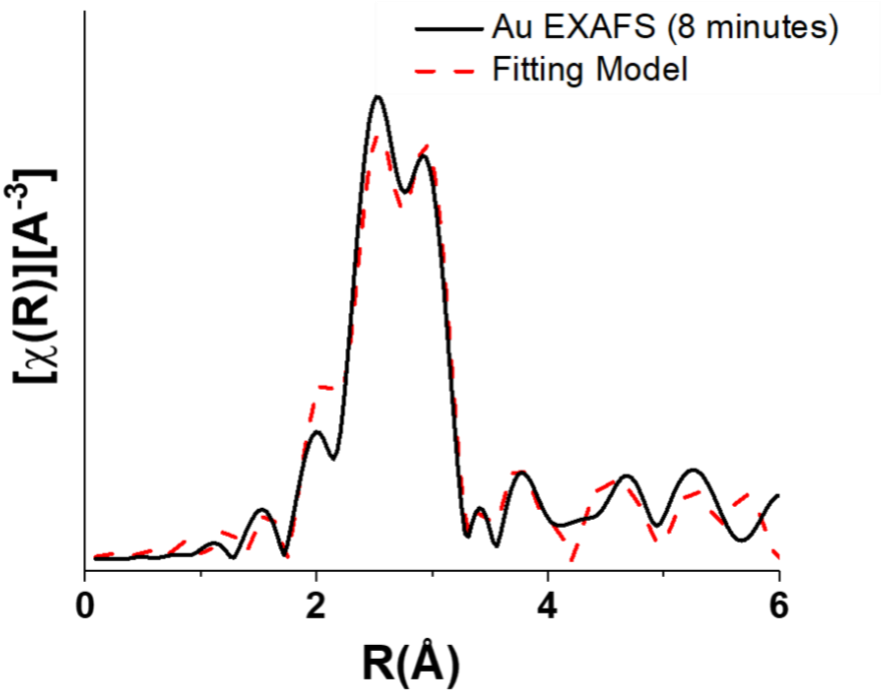

Pathway	N	R (Å)	E_0 (eV)	σ^2 (Å^2) x 10^{-3}
Au–Au (shell 1)	10.7 ± 0.9	2.858 ± 0.003	5.0 ± 0.4	7.3 ± 0.6
Au–Ag (shell 1)	1.3 ± 0.4	2.865	8.9 ± 4.4	12.5

Figure S12.12 Au K edge EXAFS spectrum and fitting model for 8 minute nanorod aliquot. The Au K-edge nanoparticle spectrum was fit using first coordination-shell atomic pathways. A fitting range from 1.5 to 4 Å and a k-range from 2 to 12 Å^{-1} was used. The R-factor parameter associated with the goodness of fit for this model was 0.02.

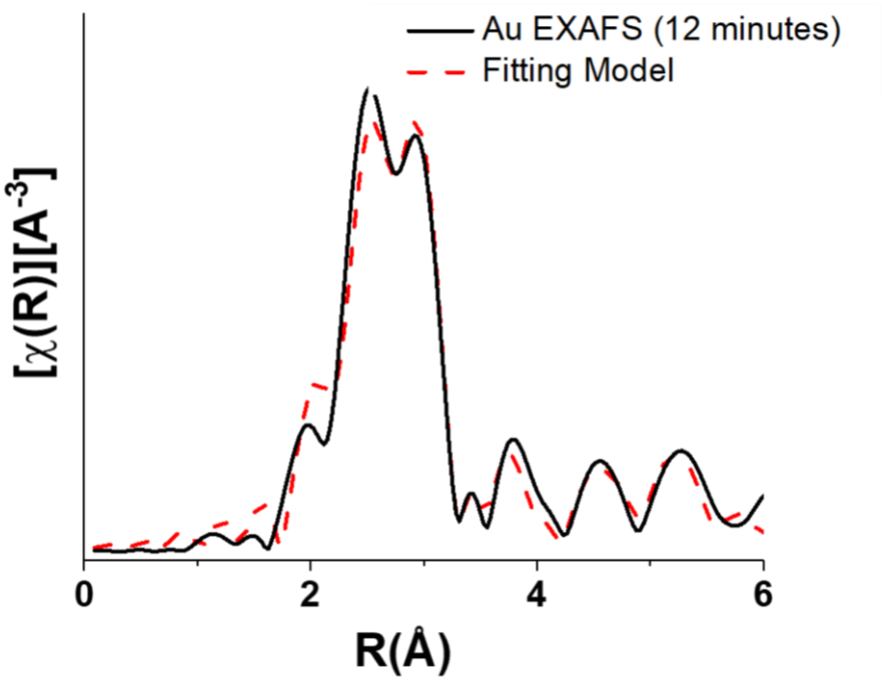

Pathway	N	R (Å)	E_0 (eV)	σ^2 (Å^2) x 10^{-3}
Au–Au (shell 1)	11.0 ± 1.3	2.859 ± 0.004	5.5 ± 0.5	10.7 ± 1.6
Au–Ag (shell 1)	1.0 ± 0.7	2.865	2.8 ± 10.6	12.6

Figure S12.13 Au L3 edge EXAFS spectrum and fitting model for 12 minute nanorod aliquot. The Au L3-edge nanoparticle spectrum was fit using first coordination-shell atomic pathways. A fitting range from 1.5 to 4 Å and a k-range from 2 to 12 Å^{-1} was used. The R-factor parameter associated with the goodness of fit for this model was 0.024.

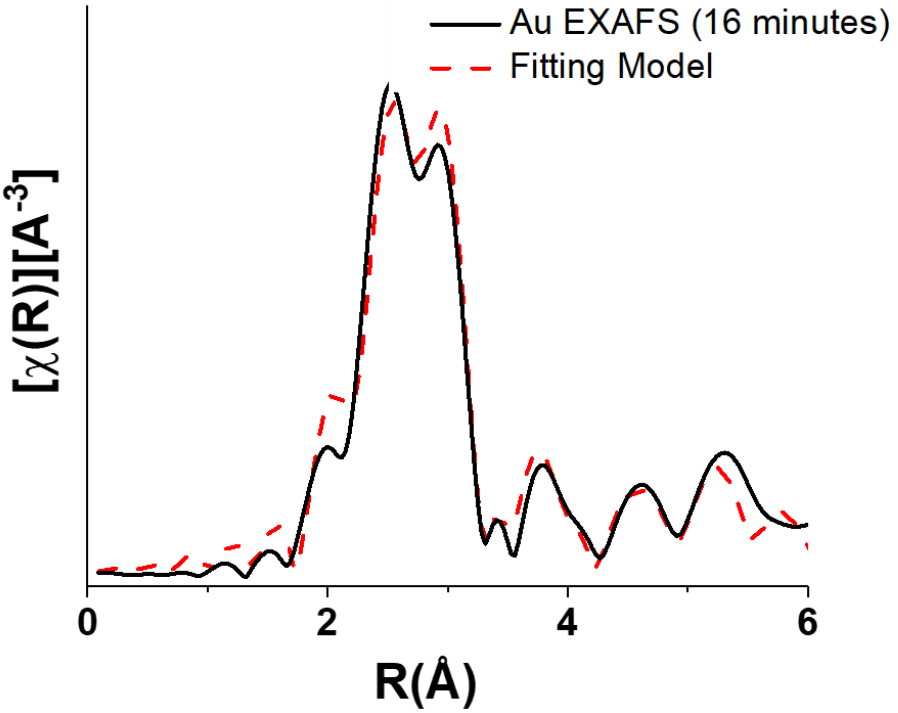

Pathway	N	R (Å)	E_0 (eV)	σ^2 (Å^2) x 10^{-3}
Au–Au (shell 1)	11.3 ± 1.1	2.859 ± 0.004	5.1 ± 0.4	7.4 ± 0.7
Au–Ag (shell 1)	0.7 ± 0.6	2.863	3.3 ± 8.9	12.4

Figure S12.14 Au K edge EXAFS spectrum and fitting model for 16 minute nanorod aliquot. The Au K-edge nanoparticle spectrum was fit using first coordination-shell atomic pathways. A fitting range from 1.5 to 4 Å and a k-range from 2 to 12 Å^{-1} was used. The R-factor parameter associated with the goodness of fit for this model was 0.018.

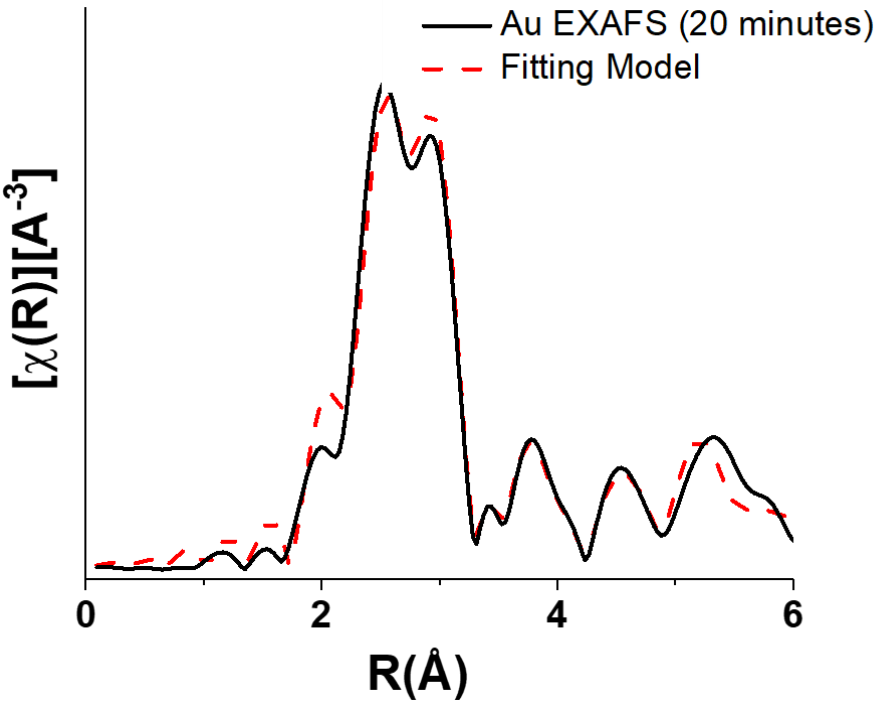

Pathway	N	R (Å)	E_0 (eV)	σ^2 (Å^2) x 10^{-3}
Au–Au (shell 1)	11.4 ± 1.0	2.859 ± 0.004	5.2 ± 0.4	7.4 ± 0.6
Au–Ag (shell 1)	0.5 ± 0.6	2.865	-0.3 ± 7.8	12.5

Figure S12.15 Au L3 edge EXAFS spectrum and fitting model for 20 minute nanorod aliquot. The Au L3-edge nanoparticle spectrum was fit using first coordination-shell atomic pathways. A fitting range from 1.5 to 4 Å and a k-range from 2 to 12 Å^{-1} was used. The R-factor parameter associated with the goodness of fit for this model was 0.015.

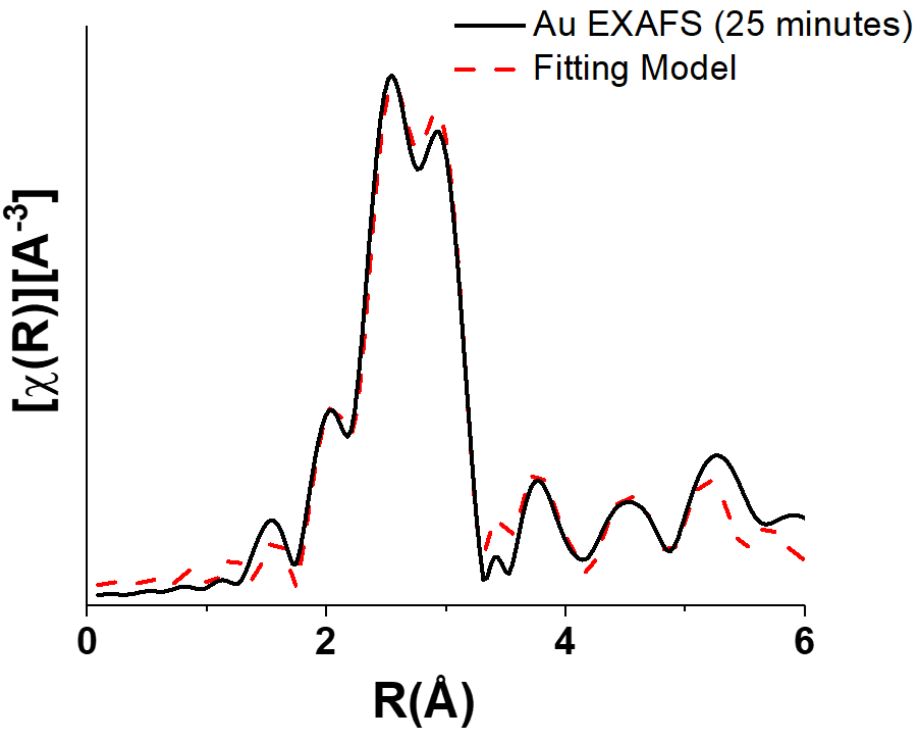

Pathway	N	R (Å)	E_0 (eV)	σ^2 (Å^2) x 10^{-3}
Au–Au (shell 1)	11.4 ± 0.8	2.860 ± 0.002	5.0 ± 0.3	7.1 ± 0.4
Au–Ag (shell 1)	0.2 ± 0.4	2.866	7.2 ± 6.2	14.4

Figure S12.16 Au L3 edge EXAFS spectrum and fitting model for 25 minute nanorod aliquot. The Au L3-edge nanoparticle spectrum was fit using first coordination-shell atomic pathways. A fitting range from 1.5 to 4 Å and a k-range from 2 to 12 Å^{-1} was used. The R-factor parameter associated with the goodness of fit for this model was 0.011.

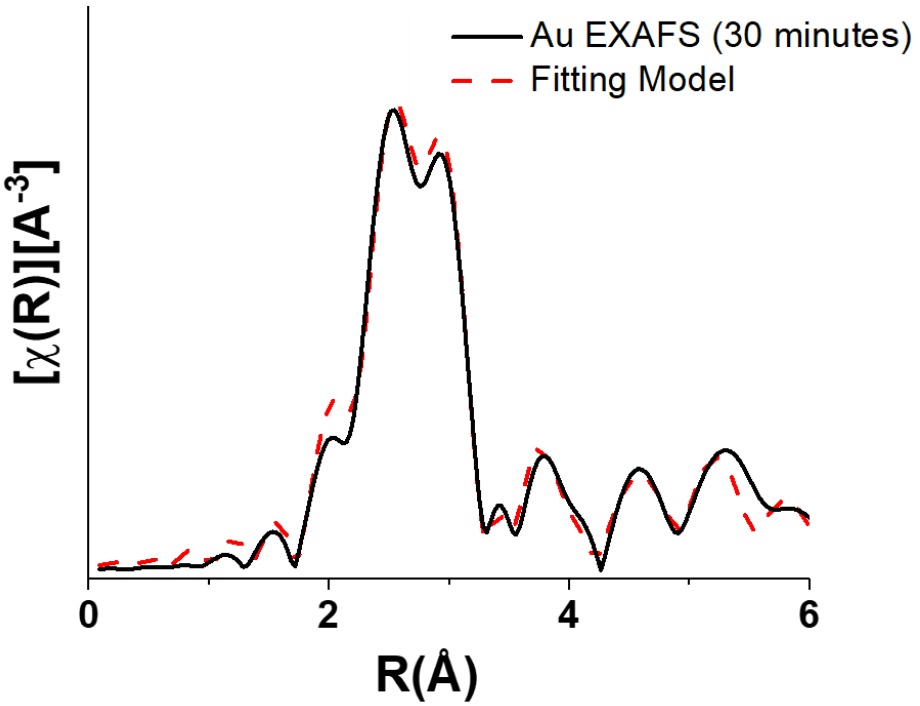

Pathway	N	R (Å)	E_0 (eV)	σ^2 (Å^2) x 10^{-3}
Au–Au (shell 1)	11.5 ± 0.8	2.858 ± 0.003	5.0 ± 0.3	7.9 ± 0.5
Au–Ag (shell 1)	0.3 ± 0.6	2.869	-9.7 ± 8.4	14.0

Figure S12.17 Au L3 edge EXAFS spectrum and fitting model for 30 minute nanorod aliquot. The Au L3-edge nanoparticle spectrum was fit using first coordination-shell atomic pathways. A fitting range from 1.5 to 4 Å and a k-range from 2 to 12 Å^{-1} was used. The R-factor parameter associated with the goodness of fit for this model was 0.009.

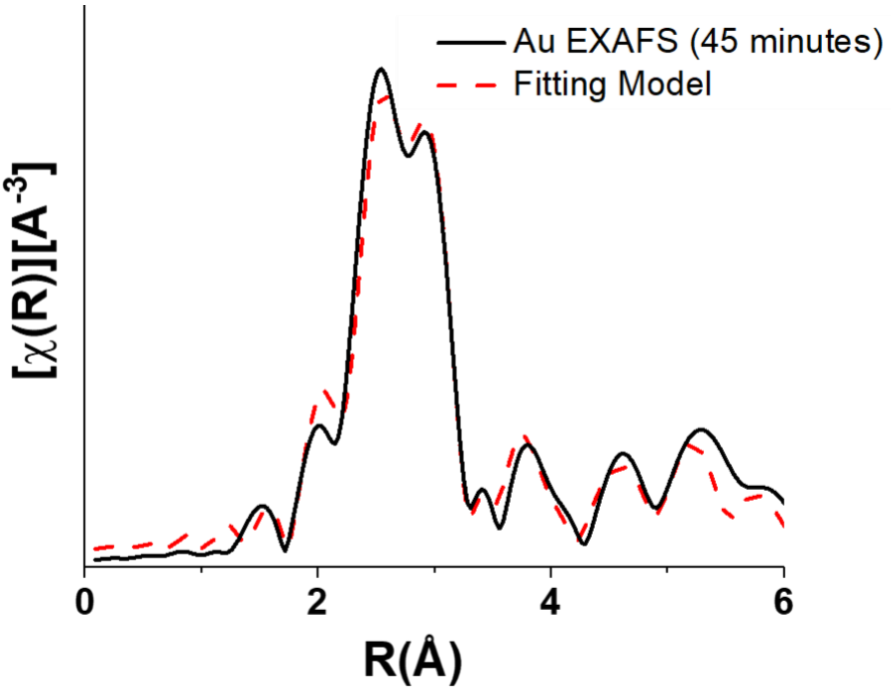

Pathway	N	R (Å)	E_0 (eV)	σ^2 (Å^2) x 10^{-3}
Au–Au (shell 1)	11.4 ± 1.0	2.859 ± 0.003	5.0 ± 0.4	7.0 ± 0.5
Au–Ag (shell 1)	0.1 ± 0.8	2.865	-8.7 ± 6.6	14.1

Figure S12.18 Au L3 edge EXAFS spectrum and fitting model for 45 minute nanorod aliquot. The Au L3-edge nanoparticle spectrum was fit using first coordination-shell atomic pathways. A fitting range from 1.5 to 4 Å and a k-range from 2 to 12 Å^{-1} was used. The R-factor parameter associated with the goodness of fit for this model was 0.014.

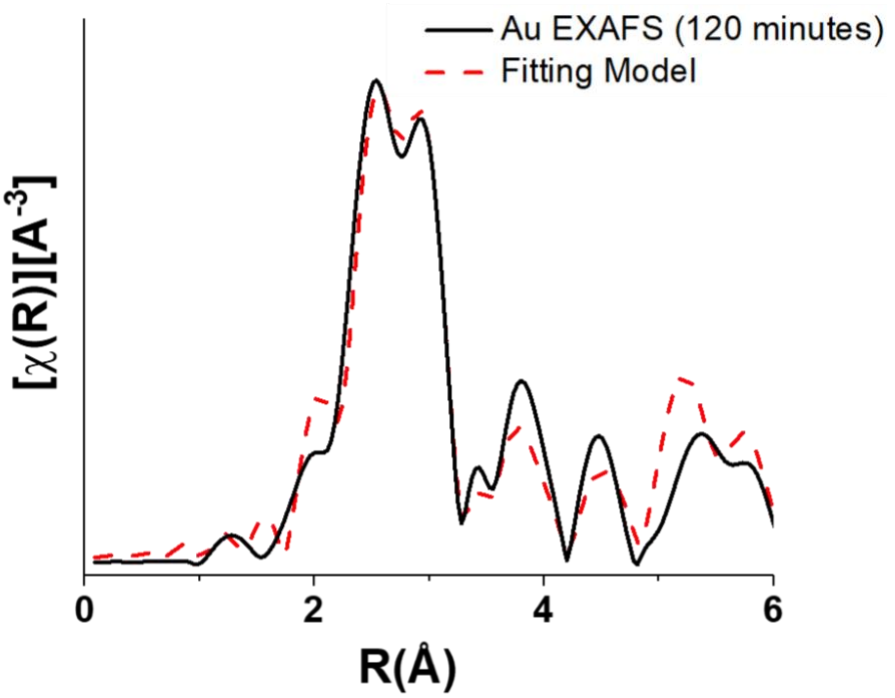

Pathway	N	R (Å)	E_0 (eV)	σ^2 (Å^2) x 10^{-3}
Au–Au (shell 1)	12.0 ± 1.3	2.857 ± 0.004	4.6 ± 0.5	6.8 ± 0.7

Figure S12.19 Au L3 edge EXAFS spectrum and fitting model for final product 120 minute nanorods. The Au L3-edge nanoparticle spectrum was fit using first coordination-shell atomic pathways. A fitting range from 1.5 to 4 Å and a k-range from 2 to 12 Å^{-1} was used. The R-factor parameter associated with the goodness of fit for this model was 0.027.

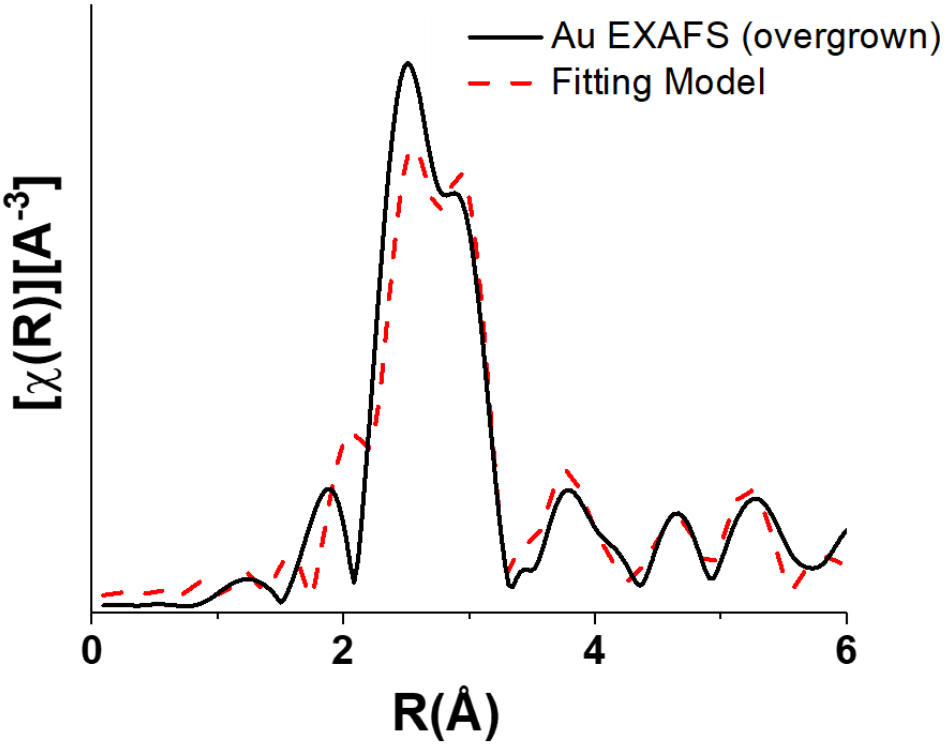

Pathway	N	R (Å)	E_0 (eV)	σ^2 (Å^2) x 10^{-3}
Au–Au (shell 1)	11.8 ± 2.4	2.861 ± 0.009	4.7 ± 1.1	7.6 ± 1.4

Figure S12.20 Au L3 edge EXAFS spectrum and fitting model for Au-overgrown nanorods. The Au L3-edge nanoparticle spectrum was fit using first coordination-shell atomic pathways. A fitting range from 1.5 to 4 Å and a k-range from 2 to 12 Å^{-1} was used. The R-factor parameter associated with the goodness of fit for this model was 0.091.

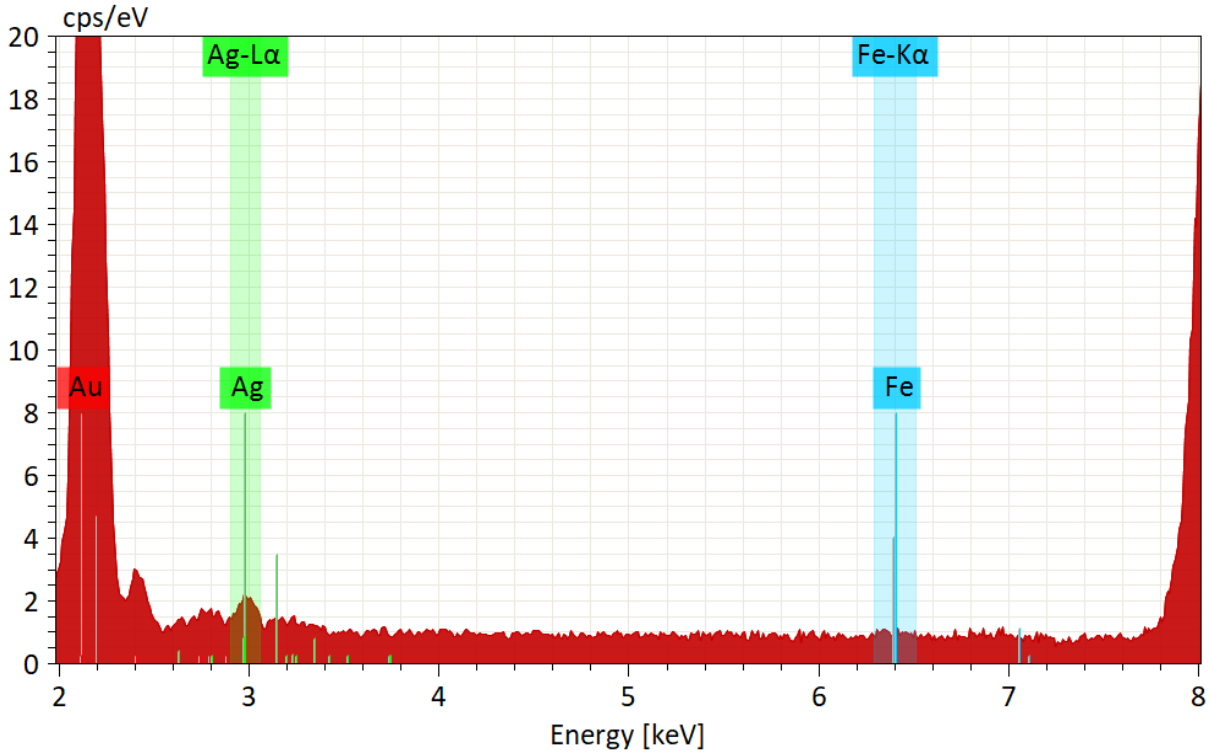

Figure S13: EDX survey spectrum sum for nanorod area highlighted in Figure 6. From the EDX spectrum, we observe that while the Ag Lα signal is lower than for the case of Au (as is expected given the high Au vs. Ag content of the nanorods), there is still a signal for Ag that is above background. In comparison, the Fe Kα signal is indistinguishable from the background. The overall low Ag signal level may contribute to the lack of determination of whether Ag is concentrated on sides of the nanorods in comparison to the tips.

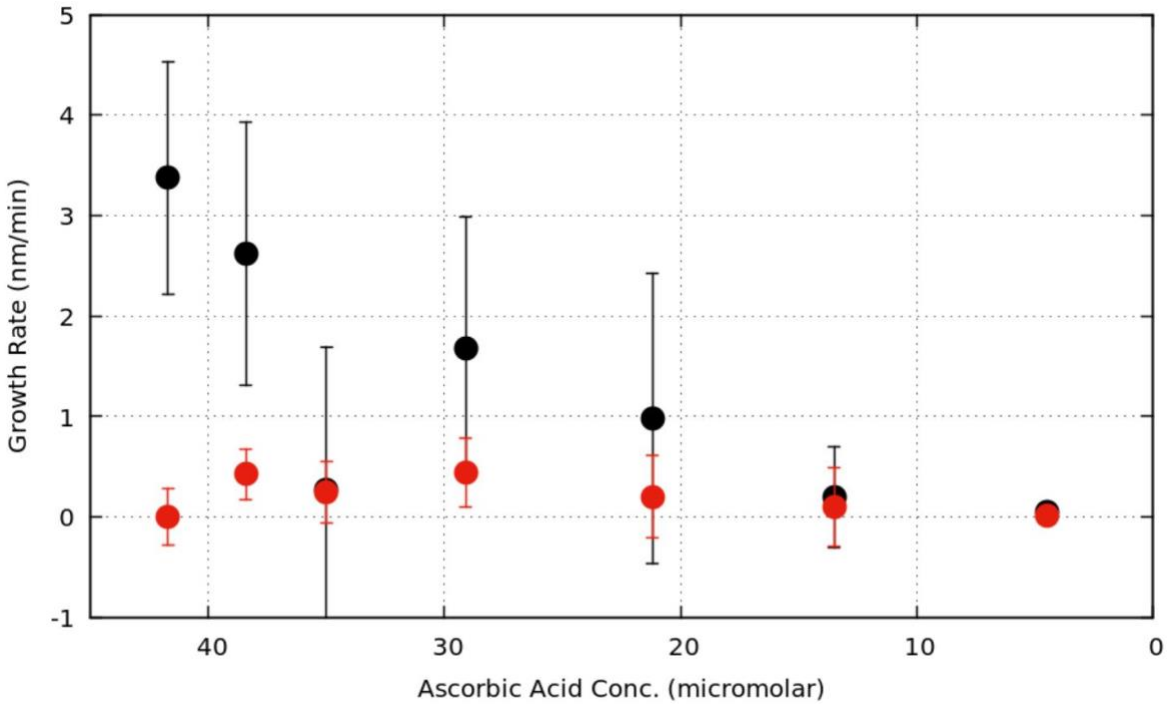

Figure S14: Relationship between nanorod length (black circle) and width (red circle) growth rate and ascorbic acid concentration in solution. If we assume that the limiting reagent in the reaction is ascorbic acid (such that at reaction completion (120 minutes) all ascorbic acid has been depleted and that each ascorbic acid molecule is able to reduce two Au^+ or Ag^+ ions (1:1 electron correlation), then the ascorbic acid concentration in solution as a function of reaction time can be calculated. When plotted along with length and width growth rates, it appears that the length growth rate may also show some correlation with ascorbic acid concentration. This can also be explained, however, by the direct relationship between the nanorod volume and ascorbic acid depletion, since larger growth rates are correlated with increasing nanorod volume and therefore increasing ascorbic acid depletion. If differences in reduction potential for Ag^+ occur as a function of ascorbic acid concentration, however, this may play a role in why the surface coverage is altered as a function of reaction time.

References

1. B. Nikoobakht and M. A. El-Sayed, *Chem. Mater.*, 2003, **15**, 1957-1962.
2. S. Puri, B. Chand, D. Mehta, M. L. Garg, N. Singh and P. N. Trehan, *Atomic Data and Nuclear Data Tables*, 1995, **61**, 289-311.
3. B. Ravel and M. Newville, *J. Synchrotron Radiat.*, 2005, **12**, 537-541.
4. B. Ravel, *J. Synchrotron Radiat.*, 2001, **8**, 314-316.
5. B. Ravel, M. Newville, J. O. Cross and C. E. Bouldin, *Physica B*, 1995, **208 & 209**, 145-147.
6. E. A. Stern, *Contemp. Phys.*, 1978, **19**, 289-310.
7. E. A. Stern, *Phys. Rev. B*, 1974, **10**, 3027-3037.
8. B. Ravel and S. D. Kelly, *AIP Conf. Proc.*, 2007, **882**, 150-152.
9. R. Scott, *Physical Methods in Bioinorganic Chemistry: Spectroscopy and Magnetism*, University Science Books, 2000.
10. A. Michalowicz and G. Vlaic, *J. Synchrotron Radiat.*, 1998, **5**, 1317-1320.
11. M. Z. Liu and P. Guyot-Sionnest, *J. Phys. Chem. B*, 2005, **109**, 22192-22200.
12. N. Almora-Barrios, G. Novell-Leruth, P. Whiting, L. M. Liz-Marzán and N. López, *Nano Lett.*, 2014, **14**, 871-875.
13. K. Park, L. F. Drummy, R. C. Wadams, H. Koerner, D. Nepal, L. Fabris and R. A. Vaia, *Chem. Mater.*, 2013, **25**, 555-563.
14. E. Carbó-Argibay, B. Rodríguez-González, S. Gómez-Graña, A. Guerrero-Martínez, I. Pastoriza-Santos, J. Pérez-Juste and L. M. Liz-Marzán, *Angew. Chem. Int. Ed.*, 2010, **49**, 9397-9400.
15. S. K. Ghosh, S. Nath, S. Kundu, K. Esumi and T. Pal, *J. Phys. Chem. B*, 2004, **108**, 13963-13971.
16. C. J. Orendorff and C. J. Murphy, *J. Phys. Chem. B*, 2006, **110**, 3990-3994.